Volume 1 | Number 1 | Jan 2013 | Pages 1–100

Journal of
Materials Chemistry A

Materials for energy and sustainability
www.rsc.org/materialsA

ROYAL SOCIETY
OF CHEMISTRY

ROYAL SOCIETY
OF CHEMISTRY

www.rsc.org/materialsA

Journal Name

Journal of Materials Chemistry A

ARTICLE TYPE

Ge/Graphene/Carbon Nanotube Composite Anode for High Performance Lithium-ion Batteries

Shan Fang, Laifa Shen, Hao Zheng, Xiaogang Zhang*

Ge/Graphene/Carbon nanotube composite electrode was constructed by germanium (Ge) nanoparticles anchor on the reduced graphene oxide (Ge/RGO) intertwined with carbon nanotubes (CNT). In this unique structure, the graphene sheets can improve electric conductivity and buffer severe volume change, additionally, the CNT, mechanically binding Ge/RGO together, to maintain the integrity of the electrodes, stabilize the electric conductive network for the active Ge nanoparticles and eventually lead to better cycling
10 performance. As a result, the designed anode exhibits an outstanding energy capacity up to 863.8 mAh g^{-1} at current density of 100 mA g^{-1} after 100 cycles and a good rate performance of 1181.7, 1073.8, 1005.2, 872.0, 767.6, and 644.8 mAh g^{-1} at current density of 100, 200, 400, 800, 1600, and 3200 mA g^{-1}, respectively. Our results indicate that the hybrids exhibit much−improved lithium storage performance.

Introduction

15 In the past decade substantial efforts have been devoted to developing rechargeable lithium−ion batteries extend to large−scale applications such as electric vehicles (EVs) and load−leveling installations on power grids. New generation electrode materials with high energy density and long cycle life have been
20 widespread studied to meet the challenging requirements of these energy storage applications.[1-5] However, existing lithium−ion batteries (LIBs) rely on anodes made from graphitic carbon that at full lithiation, only offer a theoretical capacity nearing 372 mAh g^{-1}, which is unable to satisfy the requirements for
25 increasing mobility and high energy demands.[6] Therefore, it is urgently needed to alternative anode materials with high energy and high power density for the next generation LIBs. Various anode materials with higher specific capacities have been studied in recent years.[7,8] Among them, germanium (Ge) has attracted
30 considerable interest as an anode material for next generation LIBs by virtue of its high theoretical capacity (1600 mAh g^{-1}), good lithium ion diffusivity (400 times faster than in silicon), and high electrical conductivity (104 times higher than silicon).[9,10] Although substituting Ge for graphite and the subsequent gain of
35 higher capacity have been explored previously, its major drawbacks stemming from significant volume expansion (>300%) during Li−ion insertion into Ge make it not stable enough, these lead to internal cracks and delamination from current collector and increased impedance, which seriously
40 hindered the practical application.[11−14] Various strategies have been undertaken to solve this problem, most of them are the use of nano−sized particles and carbon coating method.[15−24] Nano−sized particles could withstand mechanical strain during lithium ion insertion/extraction better than bulk and provide shorter path
45 length for the transport of lithium ion and electron.[25, 26] Thus pulverization and electrical connectivity loss caused by large

volume change of Ge could be weakened to a certain extent. The carbon coating method can protect the surface of Ge active material from exposure to the electrolyte and form a stable solid
50 electrolyte film (SEI).[27, 28] However, due to the high surface−to−volume ratio and high−surface free energy of nano materials, undesirable side reactions and agglomeration can occur easily,[29] with prolong the cycling, the uneven large volume changes of Ge during Li$^+$ insertion and extraction would destroy
55 the carbon coatings, and expose the surface of Ge to the electrolyte. Therefore, serious capacity degradation of Ge appears at the early cycles.

In order to further advancing the anode performance and stability, two−dimensional (2D) graphene or reduced graphene oxide
60 (RGO), or one−dimensional carbon nanotubes (CNT) are high priority to other carbon materials due to their many unusual features, including superior electrical conductivity, excellent mechanical flexibility, large specific surface area, and high thermal and chemical stability, which can be engineered into a
65 lightweight, robust, and flexible matrix.[30−37] For example, Hwang and co−workers fabricated Ge−MWCNT by anchoring of Ge on the surface of electrophoretically pre−deposited MWCNT networks via a thermal evaporation process. This nanocomposite electrodes obtained stable cycling performance and good rate
70 capability.[38] Cho's group directly grow graphene on a Ge NW surface by chemical vapor deposition (CVD). The Gr/Ge NW shows an excellent electrochemical performance as anode in a Li ion battery.[39] Lee and co-workers report a facile preparation of a Ge−graphene nanocomposite using a low-pressure thermal
75 evaporation approach. The nanocomposite exhibits a high Coulombic efficiency of 80.4% in the first cycle and a capacity retention of 84.9% after 400 full cycles in a half cell, along with high utilization of germanium in the composite and high rate capability.[20] Zhong's group synthesized Ge−graphene by one−
80 step aqueous − based method. The germanium−graphene

nanocomposite shows a stable cycling performance with capacity of about 832 mAh g^{-1} after 50 cycles at 0.1C. The rate capability is also improved significantly.[40] However, as so far, there is no research holds the ability to mechanically and electrically bind these nanoscale hybrid materials units together, forming a functional Ge based LIB anode.

In this paper, a comprehensive study was conducted on the Ge−based anode material (namely, Ge/RGO/CNT) consisting of Ge nanoparticles anchor on the surface of RGO and intertwined with CNT to promote the electrochemical performance of Ge based anode material for LIBs. RGO with its heavily crumpled nature is a good absorber for accommodating Ge volume changes during charge and discharge process, and is also electrically conductive, facilitating charge−transfer reactions, the tangled CNT network is expected to provide additional mechanical strength to maintain the integrity of electrodes, forming a continuous 3D electric conductive network and prevent the aggregation of Ge nanoparticles, and eventually lead to better cycling performance. The power of this concept is demonstrated by the facile synthesis of the Ge/RGO/CNT nanocomposite, which shows much improved specific capacity, cycling performance, and rate capability in comparison with pristine Ge and Ge/RGO when used as an anode material for LIBs.

Experiment Section

Preparation of Ge/RGO/CNT composites

Ge nanoparticles were synthesized according to previous literature.[41] In a typical synthesize, 1.0 mmol GeBr$_2$ and 20 ml oleylamine were added to a 50 mL three−neck flask in air, and bubbling with N$_2$ gas at ~120 °C for 30 minutes to remove moisture and oxygen. After heated the mixture at 280 °C for 4 h, a black colloidal solution was obtained. The reaction was allowed to cool to room temperature and added excess ethanol to flocculate the nanoparticles and then collected by centrifugation at 10000 rpm for 5 min. After the washing process, the precipitates were treated at 500 °C for 2 h under Ar containing 5 vol% H$_2$ atmospheres in a furnace to obtain a dark powder. The rate of heating is 2 °C min^{-1}. The Ge/RGO/CNT nanocomposite was prepared through dispersing these materials in ethanol solution. Firstly, 32 ml aqueous solution of GO was vacuum filtration and dried then ultrasonicated with 50 ml of ethanol for 2 h, which was synthesized from graphite flakes by a modified Hummers method.[42] Then, 56 mg of the prepared Ge nanoparticles and 8 mg carbon nanotube (CNT) were added into the solution under magnetic stirring for 1 h to obtain a homogeneous suspension. After that, the composites were collected by vacuum filtration washed with ethanol and dried at 60 °C for overnight. Finally, reduction in a crucible in a tube furnace at 600 °C for 4 h under 5 vol% H$_2$ atmosphere to achieve Ge/RGO/CNT products. The compared sample of Ge/RGO was fabricated by the same preparation procedure without adding CNT.

Characterization

Morphologies of the samples were characterized by scanning electron microscopy (SEM, HITACHI S−4800) and transmission electron microscopy (TEM, JEOL JEM−2010). The crystal structure was characterized by X−ray diffraction (XRD) (Bruker D8 advance) with Cu Kα radiationover the 2 Theta range of 10−80°. Raman spectra were collected using a Renishaw 2000 system with an argon ion laser (514.5 nm) and charge−coupled device detector.

Electrochemical Test

Electrochemical evaluations were tested by galvanostatic charge/discharge in a CR2016−type coin cell. 80% active materials, 10% carbon black and 10% polyvinylidene fluoride (PVDF) binder were mixed, which dissolved in N−methyl pyrrolidinone (NMP), the slurry was coated on a foil copper current collector formed as a working electrode. Then the electrodes were dried in a vacuum oven at 110 °C for overnight. The mass of active material loaded on electrode was ~0.7 mg. The cells were assembled with lithium metal as the counter electrode, polypropylene (PP) film as separator. The electrolytes were 1 mol L^{-1} LiPF$_6$ solution in a mixture of ethylene carbonate (EC) and dimethyl carbonate (DMC) (1:1, by volume). All the cells were assembled inside an argon−filled glove box. Galvanostatically charge/discharge experiments were tested at the voltage between 0.01 and 2.0 V (vs. Li/Li$^+$) using a CT2001A cell test instrument (LAND Electronic Co.). An electrochemical workstation (CHI660) was used to study the cyclic voltammetry (CV) performance in the potential range of 0.05−2.0 V at a scan rate of 0.1 mV s^{-1}. Electrochemical impedance spectroscopy (EIS) was measured in the frequency between 100 kHz and 0.01 Hz and the amplitude is 5 mV.

Results and Discussions

The overall synthetic process for the continuous 3D electric conductive network of Ge/RGO/CNT nanocomposite is schematized in Fig. 1. A solution method based on the reaction between GeBr$_2$ and oleylamine are used to prepare Ge NPs as reported previously.[41] The as−obtained Ge NPs are first heat treatment at 500 °C for 2 h under Ar to get a dark powder. Then added into the ethanol solution of graphene oxide (GO) which was synthesized according to the modified Hummer's method starting from graphite powder. Acid−treated carbon nanotubes can be well dispersed in ethanol solutions, the individual CNT are adsorbed onto the surface of GO sheets due to the p−stacking interactions and the reactions of oxygen functionalities such as hydroxyl, carbonyl and carboxyl groups or other defects in the oxidized graphitic structures. Finally, the products were obtained by vacuum filtration and heating at 600 °C for 4 h under Ar containing 5% H$_2$ in order to reduce GO into RGO. To investigate structure of the composite, we first perform the scan electron microscopy (SEM) analysis on the composite samples as shown in Fig. 2. The Ge nanoparticles in both Ge/RGO and Ge/RGO/CNT samples were well wrapped by graphene. Unwrapped Ge nanoparticles were not observed, suggesting high yield of graphene−encapsulated Ge composite in the fabricated process. From Fig. 2c and d, we can easily find the CNT inserted between RGO sheets and Ge nanoparticles, thus preventing Ge nanoparticles from aggregation. This unique nano−structure of
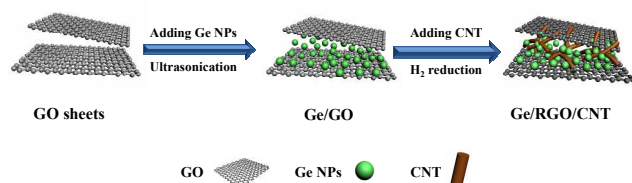
Fig. 1. Schematic illustration of the preparation process of the Ge/RGO/CNT nanocomposite.

the Ge/RGO/CNT not only improves the electronic conductivity
5 of active materials, but also provides void space to accommodate the volume changes of Ge nanoparticles during charge/discharge cycles, maintaining high electronic conductivity of the composite. These hybrid carbon conducting fillers, namely graphene sheets and CNTs were employed to achieve the synergy effects of
10 forming extensive 3D conducting networks that cannot be obtained using one type of carbon fillers alone.
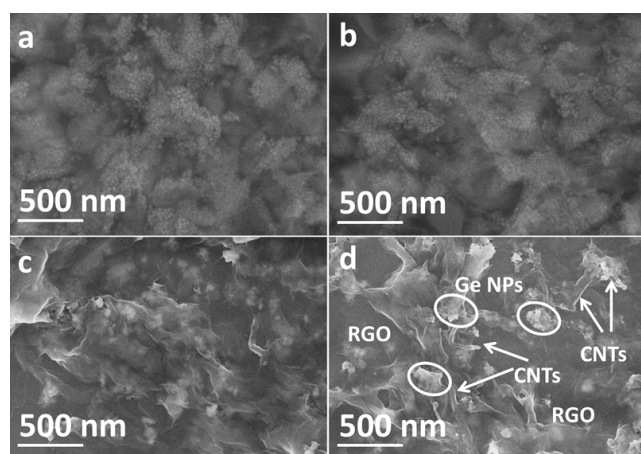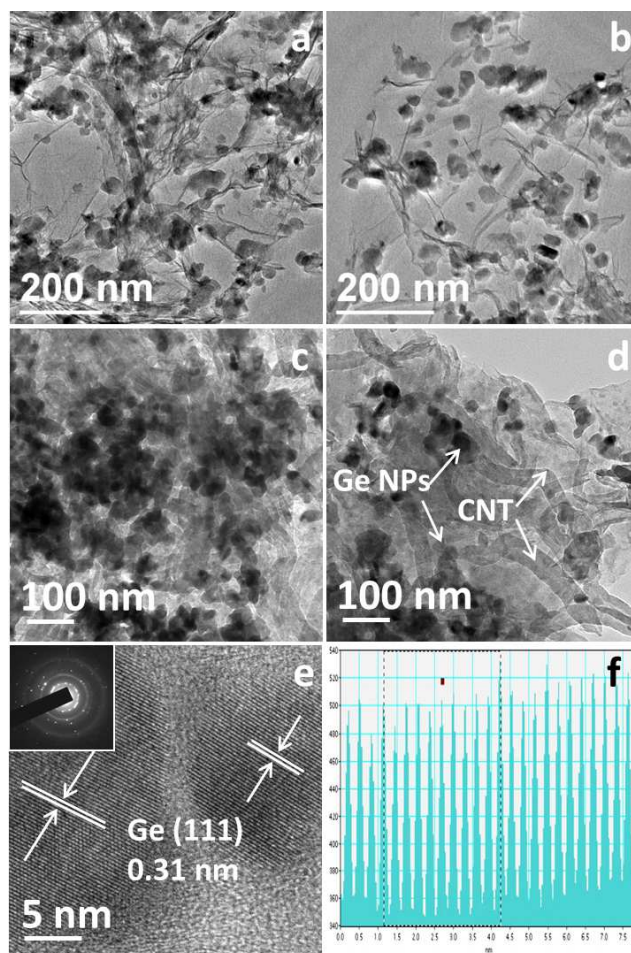

Fig. 2. SEM images of (a, b) Ge/RGO, (c, d) Ge/RGO/CNT nanocomposite.

15 To further study the morphology of the materials, transmission electron microscopy (TEM) was used to analyze the materials. From the TEM images (Fig. 3a, b), both the Ge NPs and transparent layers can be observed clearly, and the Ge NPs with the diameters in the range of $20-30$ nm were uniformly
20 distributed on the graphene substrate, avoiding/weakening the loss of their high active surface area. The images shown in Fig. 3c and d reveal that the individual CNT were placed on the graphene surface together with surrounding Ge nanoparticles, indicating that both the graphene and CNTs in the hybrids were
25 effectively distributed in the Ge/RGO/CNT hybrid sample. Therefore, constructing the RGO/CNT hierarchical structure effectively prevented the stacking of graphene sheets and aggregation of Ge nanoparticles, leading to higher porosity and larger specific surface area to enhance the electrochemical
30 performances of Ge/RGO/CNT. Also, the conductive CNT wraps around Ge/RGO to provide an additional electron−transport path besides the graphene layer underneath of Ge nanoparticles, and improving the electrode integrity, thus mitigating the destruction of the electric network even under a large volume change during
35 cycling. The high transmission electron microscopy (HRTEM) analysis exhibits the lattice fringe that is indicative of the well−crystallized Ge (Fig. 3e). The calculated interference fringe

spacing of Ge is about 0.31 (Fig. 3f), which is agree well with the (111) plane of diamond cubic Ge. The selected−area electron
40 diffraction (SAED) pattern (inset of Fig. 3e) also reveals that the nanoparticles have a diamond cubic structure.

The crystal structures of the Ge nanoparticles, Ge/RGO and Ge/RGO/CNT samples were characterized by X−ray diffraction (XRD), as shown in Fig. 4a. All the reflection peaks of the
45 samples are well indexed to diamond cubic phase (Ge) (JCPDS card No. 04−0545). There are no peaks corresponding to carbon

Fig. 3. TEM images of (a, b) Ge/RGO, (c, d) Ge/RGO/CNT nanocomposite. (e, f) HRTEM of Ge nanoparticles (Inset: selected area
50 SAED pattern for Ge nanoparticles and the correspond calculation of interference fringe spacing.

have been detected in the pattern, which could be attributed to their overlapping with the (111) peak of germanium at around 27°. To investigate the carbon quality of the synthesized RGO
55 sheets, we obtained Raman spectrum (Fig. 4b). The RGO exhibits two peaks around 1348.1 and 1584.9 cm^{-1}, which are attributed to the D and G bands of carbon, respectively. The D band corresponds to the structural defects and disorder of carbon, while the G band corresponds to the stretching vibration mode of
60 graphite crystals. A stronger D band is observed than G band, indicating a largely disordered structure of the obtained RGO.
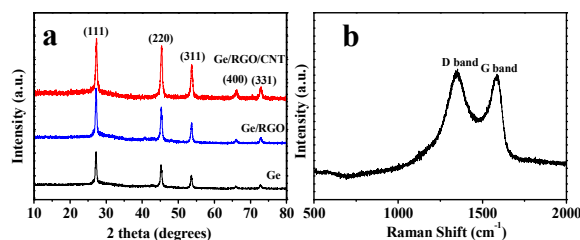
Fig. 4. (a) XRD patterns of Ge, Ge/RGO and Ge/RGO/CNT. (b) Raman spectrum of the as−prepared RGO sheets.

A series of electrochemical characterizations were carried out to investigate the electrochemical properties of the composite electrodes in a coin−type half−cell (2016 type). The electrochemical properties of Ge nanoparticles, Ge/RGO and Ge/RGO/CNT were evaluated and compared (Fig. 5). Fig. 5a shows the charge/discharge voltage profiles of the three samples at a current density of 100 mA g^{-1} in the voltage between 0.01 and 2.0 V. It is evident that the discharge process of the three samples consists of three stages: the first stage is the quick voltage drop, the second stage is the distinct voltage plateau, and the third stage is a gradual decay in potential. A distinct plateau at about 0.3 V can be observed and this should be attributed to the lithium alloying with crystalline Ge nanoparticles.[43] The initial discharge and charge capacities of Ge nanoparticles are 1765.1 and 696.4 mAh g^{-1}, respectively, corresponding to a Coulombic efficiency (CE) of 39.4%. The relatively low initial CE of pristine Ge can be attributed to the drastic volume changes and the loss of electric contact between Ge nanoparticles, which in turn leads to large irreversible capacity. The charge/discharge curves of Ge/RGO are also shown in Fig. 5a. In addition to the potential plateau at 0.3 V, an obvious step can also be observed between 0.70 and 0.30 V is attributed to solid electrolyte interphase (SEI), which is formed by the irreversible decomposition of electrolyte on the surface of the electrode material.[44, 45] The initial discharge and charge capacity of Ge/RGO are 1563.2 and 1208.2 mAh g^{-1}, respectively, corresponding to a CE of 77.3%. It should be noted that the CE is improved after adding RGO even if an obvious irreversible SEI formation process is observed between 0.70 and 0.30 V, which should be attributed to the volume buffer effect of reduced graphene oxide and the better electric conductive network. The Ge/RGO/CNT (Fig. 5a) shows a similar charge/discharge characteristic to that of Ge/RGO. The initial discharge and charge capacities of Ge/RGO/CNT are 1602.4 and 1277.4 mAh g^{-1}, respectively. And the CE is up to 79.7%. Apparently, the 3D conducted network structure resulted in profound improvement in electrochemical performance.

The cycling behaviors for the three different samples are shown in Fig. 5b. Here, all capacities were calculated on the basis of the total weight of composite material including Ge, graphene and CNT. The discharge capacity of the pristine Ge electrode rapidly decreased to a capacity of 220 mAh g^{-1} after 100 cycles at a current density of 100 mA g^{-1}, this may originate from the serious pulverization of the Ge, during which the SEI layer continuously ruptures and reforms, consuming Li^{+}. In comparison, the 3D conductive network form by graphene and CNT grafted Ge composites still retain a specific discharge

capacity of about 863.8 mAh g^{-1}. It is worthwhile to point out that even without adding CNT, the composites of Ge/RGO still showed improved cycle performance compared to bare Ge nanoparticles, but a worse cycle life performance than that of the Ge/RGO/CNT. This result may ascribe to the three−dimensional electric conductive network can improve the electric conductivity and buffer the volume change and the CNTs work together to achieve high electrode integrity. In order to confirm the reaction mechanism of alloying/de−alloying for Ge/RGO/CNT, cyclic voltammetry (CV) was conducted on the cell with Ge/RGO/CNT at ambient temperature in the range of 0.05−2.0 V at a scan rate of 0.1 mV s^{-1}. Li metal was used as the counter electrode. The CV curves of the first three cycles are shown in Fig. 5c. Two extra reduction peaks at 1.47 and 0.68 V were observed in the first scanning cycle, which could be associated with the formation of a solid electrolyte interphase (SEI) layer. The other two peaks are present at 0.24 and 0.09 V, indicating the complete reduction process. However, both of them have disappeared after the second cycle,[46] and new, well−defined peaks arise at 0.49, 0.33, and 0.11 V.[47,48] These are stable and detectable, suggesting a multi−step lithium insertion mechanism, because the electrochemical reaction of Ge with lithium exhibits multiple peaks during repeated lithiation, indicating the presence of successive Li phase transformations, as follows: Ge→Li$_9$Ge$_4$→Li$_7$Ge$_2$→Li$_{15}$Ge$_4$→Li$_{22}$Ge$_5$.[48] Moreover, the positions and intensities of the redox peaks remained unchanged during the second and third cycles, thus suggesting that the Ge/RGO/CNT nanocomposite electrode has excellent electrochemical reversibility.
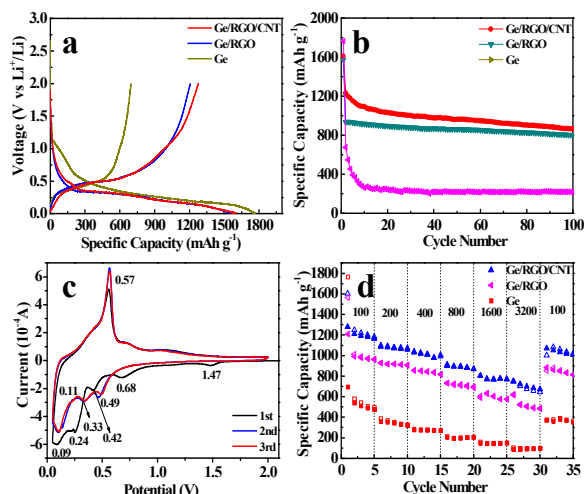
Fig. 5. (a) Charge/discharge voltage profiles of pure Ge, Ge/RGO and Ge/RGO/CNT nanocomposite at a rate of 100 mA g^{-1}. (b) Cycling performance of the three different samples at a current density of 100 mA g^{-1}. (c) Cyclic voltammetry curves of Ge/RGO/CNT between 2.0 and 0.05 V with a scan rate of 0.1 mV s^{-1}. (d) Rate performance of pure Ge, Ge/RGO and Ge/RGO/CNT nanocomposite electrodes at different current rates.

The fast discharge/charge further validates the reliability of RGO/CNT conductive network during a rapid substantial expansion and contraction for Ge nanoparticles. The rate performances of Ge nanoparticles, Ge/RGO, Ge/RGO/CNT at the current density of 100−3200 mA g^{-1} are compared in Fig. 5d.

Remarkably, as the discharge/charge rate increased from 100 to 3200 mA g^{-1}, the capacities of pure Ge decreased steeply, whereas the Ge/RGO mixture decreased relatively slower at the same rate. By introducing conductive CNT inserted into Ge/RGO to form a 3D conductive network structure, Ge/RGO/CNT hybrid nanostructures exhibited the highest rate capacity among the three samples. It is noteworthy that the capacity (754.1 mAh g^{-1}) obtained by Ge/RGO/CNT nanocomposite at a current density of 3200 mA g^{-1} is higher than that obtained at a current density of 100 mA g^{-1} for the bare Ge (496.2 mAh g^{-1}) and 1600 mA g^{-1} for the Ge/RGO mixture (686.3 mAh g^{-1}). Our Ge/RGO/CNT hybrid
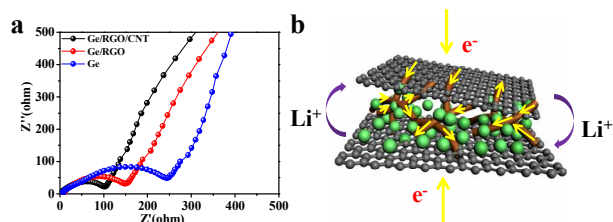
Fig. 6. (a) Nyquist plots of the electrodes of Ge, Ge/RGO and Ge/RGO/CNT nanocomposites. (b) Schematic drawing of Ge/RGO/CNT nanocomposites electrode.

nanostructures have better electrochemical properties than graphene−wrapped Ge nanoparticle [49] and Germanium−graphene nanocomposite synthesized by reduced GeO$_2$.[40]

To confirm the enhanced electrical conductivity of the Ge/RGO/CNT in comparison with Ge/RGO and Ge nanoparticles, we performed electrochemical impedance spectroscopy (EIS) measurement of the three electrodes after running 100 cycles at the same current density. The EIS spectra for the three electrodes are typically consist of a depressed semicircle in the high−frequency region and an inclined line in the low−frequency region are shown in Fig. 6a. The depressed semicircle mainly consists of the interfacial charge transfer impedance (R_{ct}) at the medium−to−high frequency range although high−frequency SEI film impedance (R_{SEI}) contributes to it. The inclined line corresponds to the lithium ion diffusion impedance. Apparently, the Ge/RGO/CNT electrode shows a much lower charge−transfer resistance R_{ct} and R_{SEI} than does the Ge/RGO and Ge NPs electrodes, indicating faster Li−ion migration through the SEI film and faster charge−transfer reaction for the Ge/RGO/CNT anode, resulting in the better rate capability and higher reversible capacity in comparison with the pure Ge nanoparticles, which is similar to the phenomenon found in many other graphene−based hybrids. The characteristics of Ge/RGO/CNT anode in LIBs are elucidated by the schematic diagram (Fig. 6b). The high specific capacity and superior rate capability of Ge/RGO/CNT are closely related to its unique structure, which favors both the ion and electron transportation in the LIBs. First, the small size (20−30 nm) and uniform distribution of germanium nanoparticles between the graphene and the CNT interconnected network promote fast lithium ion diffusion and further improve the conductivity of the composite. Second, the CNT attached on the surface of grapheme reduces the π−π interaction between graphene sheets resulting from steric hindrance, resulting in reducing the degree of restacking of RGO and consequently keeping their large active contact area between

the electrode and electrolyte, which leads to a decrease of the current density per unit surface area and an increase in the charge/discharge rate. Third, the high structural stability of the composite material owing to the synergistic effects of the graphene sheets and CNTs which intertwined the germanium nanoparticles protects them from peeling off and further pulverization. The CNT inserted in the RGO sheets could provide a support for anchoring well−dispersed Ge, the three−dimensional interconnected network possesses continuous electronic conductivity and Li diffusivity, which are favorable in terms of its LIB performance.

Conclusions

In summary, we have developed a facile route to form a 3D continue conductive network structure as an advanced anode material for high−power LIBs. The Ge nanoparticles were uniformly dispersed on the surface of graphene and carbon nanotubes, which serve as the ideal host for fast and efficient lithium storage. The highly conductive 3D networks formed by the interlaced carbon nanotubes intimately embedded or attached on the graphene, which serves as a highly conductive substrate that is beneficial to the high−rate performance. At the same time, the large surface area provides more reaction sites and lower activation energy for lithium ion insertion/extraction. It is believed that such hybrid materials composed of nanoactive particles (0D), carbon nanotubes (1D), and graphene (2D) with designed structure and varied properties will be useful in energy storage and other important applications.

Acknowledgements

Notes and references

Jiangsu Key Lab of Material and Technology for Energy Conversion, College of Materials Science and Engineering, Nanjing University of Aeronautics and Astronautics, Nanjing, 210016, P.R. China
Corresponding author Tel: +86 025 52112902; Fax: +86 025 52112626.
E-mail address: azhangxg@nuaa.edu.cn

† Electronic Supplementary Information (ESI) available: [details of any supplementary information available should be included here]. See DOI: 10.1039/b000000x/

1.　X. Zhou, Z. Dai, S. Liu, J. Bao and Y. G. Guo, *Advanced Materials (Deerfield Beach, Fla.)*, 2014, **26**, 3943-3949.
2.　L. Zhang, H. B. Wu, B. Liu and X. W. Lou, *Energy & Environmental Science*, 2014, **7**, 1013-1017.
3.　Z. Liang, G. Zheng, W. Li, Z. W. Seh, H. Yao, K. Yan, D. Kong and Y. Cui, *Acs Nano*, 2014, **8**, 5249-5256.
4.　M. S. Park, E. Park, J. Lee, G. Jeong, K. J. Kim, J. H. Kim, Y. J. Kim and H. Kim, *ACS applied materials & interfaces*, 2014, **6**, 9608-9613.
5.　X. Huang, H. Yu, J. Chen, Z. Lu, R. Yazami and H. H. Hng, *Advanced Materials*, 2014, **26**, 1296-1303.

6. M. Armand and J. M. Tarascon, *Nature*, 2008, **451**, 652-657.

7. M. J. Armstrong, C. O'Dwyer, W. J. Macklin and J. D. Holmes, *Nano Research*, 2014, **7**, 1-62.

8. B. L. Ellis, P. Knauth and T. Djenizian, *Advanced Materials (Deerfield Beach, Fla.)*, 2014, **26**, 3368-3397.

9. G. Cui, L. Gu, L. Zhi, N. Kaskhedikar, P. A. van Aken, K. Muellen and J. Maier, *Advanced Materials*, 2008, **20**, 3079-3083.

10. K. H. Seng, M.-H. Park, Z. P. Guo, H. K. Liu and J. Cho, *Angewandte Chemie-International Edition*, 2012, **51**, 5657-5661.

11. X. H. Liu, Y. Liu, A. Kushima, S. Zhang, T. Zhu, J. Li and J. Y. Huang, *Advanced Energy Materials*, 2012, **2**, 722-741.

12. C. K. Chan, H. Peng, G. Liu, K. McIlwrath, X. F. Zhang, R. A. Huggins and Y. Cui, *Nature Nanotechnology*, 2008, **3**, 31-35.

13. L. Y. Beaulieu, K. W. Eberman, R. L. Turner, L. J. Krause and J. R. Dahn, *Electrochemical and Solid State Letters*, 2001, **4**, A137-A140.

14. B. Key, R. Bhattacharyya, M. Morcrette, V. Seznec, J. M. Tarascon and C. P. Grey, *Journal of the American Chemical Society*, 2009, **131**, 9239-9249.

15. T. Kennedy, E. Mullane, H. Geaney, M. Osiak, C. O'Dwyer and K. M. Ryan, *Nano Letters*, 2014, **14**, 716-723.

16. C. H. Kim, H. S. Im, Y. J. Cho, C. S. Jung, D. M. Jang, Y. Myung, H. S. Kim, S. H. Back, Y. R. Lim, C. W. Lee, J. Park, M. S. Song and W. I. Cho, *Journal of Physical Chemistry C*, 2012, **116**, 26190-26196.

17. Y. D. Ko, J. G. Kang, G. H. Lee, J. G. Park, K. S. Park, Y. H. Jin and D. W. Kim, *Nanoscale*, 2011, **3**, 3371-3375.

18. H. Lee and J. Cho, *Nano Letters*, 2007, **7**, 2638-2641.

19. L. Li, K. H. Seng, C. Feng, H. K. Liu and Z. Guo, *Journal of Materials Chemistry A*, 2013, **1**, 7666-7672.

20. J. G. Ren, Q. H. Wu, H. Tang, G. Hong, W. Zhang and S. T. Lee, *Journal of Materials Chemistry A*, 2013, **1**, 1821-1826.

21. C. Wang, J. Ju, Y. Yang, Y. Tang, J. Lin, Z. Shi, R. P. S. Han and F. Huang, *Journal of Materials Chemistry A*, 2013, **1**, 8897-8902.

22. J. Wang, J. Z. Wang, Z. Q. Sun, X. W. Gao, C. Zhong, S. L. Chou and H. K. Liu, *Journal of Materials Chemistry A*, 2014, **2**, 4613-4618.

23. Y. Xiao, M. Cao, L. Ren and C. Hu, *Nanoscale*, 2012, **4**, 7469-7474.

24. G. Jo, I. Choi, H. Ahn and M. J. Park, *Chemical Communications*, 2012, **48**, 3987-3989.

25. H. Wu and Y. Cui, *Nano Today*, 2012, **7**, 414-429.

26. X. L. Wu, Y. G. Guo and L. J. Wan, *Chemistry-an Asian Journal*, 2013, **8**, 1948-1958.

27. K. Karki, Y. Zhu, Y. Liu, C. F. Sun, L. Hu, Y. Wang, C. Wang and J. Cumings, *ACS Nano*, 2013, **7**, 8295-8302.

28. M. E. Stournara, Y. Qi and V. B. Shenoy, *Nano Letters*, 2014, **14**, 2140-2149.

29. B. Jang, M. Park, O. B. Chae, S. Park, Y. Kim, S. M. Oh, Y. Piao and T. Hyeon, *Journal of the American Chemical Society*, 2012, **134**, 15010-15015.

30. H. Gwon, H.-S. Kim, K. U. Lee, D.-H. Seo, Y. C. Park, Y.-S. Lee, B. T. Ahn and K. Kang, *Energy & Environmental Science*, 2011, **4**, 1277-1283.

31. L. Hu, J. W. Choi, Y. Yang, S. Jeong, F. La Mantia, L. F. Cui and Y. Cui, *Proceedings of the National Academy of Sciences of the United States of America*, 2009, **106**, 21490-21494.

32. X. Peng, L. Peng, C. Wu and Y. Xie, *Chemical Society Reviews*, 2014, **43**, 3303-3323.

33. J. Yan, T. Wei, Z. J. Fan., W. Z. Qian, M. L. Zhang, X. D. Shen, and F. Wei, *Journal of Power Sources*, 2010, **195**, 3041-3045.

34. W. J. Lee, T. H. Hwang, J. O. Hwang, H. W. Kim, J. Lim, H. Y. Jeong, J. Shim, T. H. Han, J. Y. Kim, J. W. Choi and S. O. Kim, *Energy & Environmental Science*, 2014, **7**, 621-626.

35. W. Wang, S. Guo, M. Penchev, I. Ruiz, K. N. Bozhilov, D. Yan, M. Ozkan and C. S. Ozkan, *Nano Energy*, 2013, **2**, 294-303.

36. B. Zhang, Q. B. Zheng, Z. D. Huang, S. W. Oh and J. K. Kim, *Carbon*, 2011, **49**, 4524-4534.

37. J. D. Ocon, J. K. Lee, J. Lee, *Applied Chemistry for Engineering*, 2014, **25**, 1-13.

38. I. S. Hwang, J. C. Kim, S. D. Seo, S. Lee, J. H. Lee and D. W. Kim, *Chemical Communications*, 2012, **48**, 7061-7063.

39. H. Kim, Y. Son, C. Park, J. Cho and H. C. Choi, *Angewandte Chemie-International Edition*, 2013, **52**, 5997-6001.

40. C. Zhong, J.-Z. Wang, X.-W. Gao, D. Wexler and H.-K. Liu, *Journal of Materials Chemistry A*, 2013, **1**, 10798-10804.

41. D. J. Xue, S. Xin, Y. Yan, K. C. Jiang, Y. X. Yin, Y. G. Guo and L. J. Wan, *Journal of the American Chemical Society*, 2012, **134**, 2512-2515.

42. W. S. Hummers, R. E. Offeman, *Journal of the American Chemical Society*, 1958, **80**, 1339–1339.

43. C. K. Chan, X. F. Zhang and Y. Cui, *Nano Letters*, 2008, **8**, 307-309.

44. J. Graetz, C. C. Ahn, R. Yazami and B. Fultz, *Journal of the Electrochemical Society*, 2004, **151**, A698-A702.

45. Y. M. Lee, J. Y. Lee, H.-T. Shim, J. K. Lee and J.-K. Park, *Journal of the Electrochemical Society*, 2007, **154**, A515-A519.

46. W. Li, J. Zheng, T. Chen, T. Wang, X. Wang and X. Li, *Chemical Communications*, 2014, **50**, 2052-2054.

47. J. Wang, N. Du, H. Zhang, J. Yu and D. Yang, *Journal of Materials Chemistry*, 2012, **22**, 1511-1515.

48. B. Laforge, L. Levan-Jodin, R. Salot and A. Billard, *Journal of the Electrochemical Society*, 2008, **155**, A181-A188.

49. J. Cheng and J. Du, *Crystengcomm*, 2012, **14**, 397-400.

Ge/Graphene/Carbon Nanotube Composite Anode for High Performance Lithium-ion Batteries

5 *Shan Fang, Laifa Shen, Hao Zheng, Xiaogang Zhang**

Ge/Graphene/Carbon nanotube composite electrode was constructed by germanium (Ge) nanoparticles anchor on the reduced graphene oxide (Ge/RGO) and intertwined with carbon nanotubes (CNT). The composite exhibits high rate capability and cycle stablity, which is ascribe to the graphene sheet can improve electric conductivity and buffer the severe volume change, additionally, the CNT, mechanically binding Ge/RGO together, to maintain the
10 integrity of the electrodes, stabilize the electric conductive network for the active Ge nanoparticles.